Available online at www.sciencedirect.com
SCIENCE DIRECT
Journal of volcanology and geothermal research
Journal of Volcanology and Geothermal Research 155 (2006) 227–243
www.elsevier.com/locate/jvolgeores

Sub-recent volcanism in Northern Patagonia: A tectonomagmatic approach

Gabriela I. Massaferro [a,b,*], Miguel J. Haller [a,b,1], Massimo D'Orazio [c], Viviana I. Alric [a,b]

[a] Universidad Nacional de la Patagonia San Juan Bosco, Bvd. Brown 3700, 9210 Puerto Madryn, Argentina
[b] Centro Nacional Patagónico, CONICET, Bvd. Brown 3500, 9120 Puerto Madryn, Argentina
[c] Dipartamento de Scienze della Terra, Universitá di Pisa, Via S. Maria, 53, Pisa, Italy

Received 22 July 2005; received in revised form 29 January 2006; accepted 2 February 2006

Abstract

The Crater Basalt Volcanic Field (CBVF) in northern Patagonia (~42°S, Chubut province) is located 400 km eastward of the current Peru–Chile Trench and to the southwest of the Meseta de Somuncura, in a back-arc position in the extra-Andean Patagonia. The CBVF lava flows cover glaciation related terraces and present stream valleys. The occurrence of CBVF is related with the Gastre Fault System (GFS), a very significant tectonic feature about 40 km wide.

The CBVF volcanics cover a surface of ~700 km^2, occurring mainly as lava flows and scoria cones. CBVF volcanics have relatively high contents of MgO (6–9 wt.%), Cr (136–289 ppm) and Ni (25–198 ppm), and classify as alkali basalts, basanites and trachybasalts. Geothermometry indicates a crystallization temperature of ~1140 °C and a fO_2 of −1.0 1 to 0.0 (log FMQ units).

The petrographic and geochemical characteristics of CBVF products suggest that the magma originated from a garnet-bearing lherzolite mantle source with asthenospheric characteristics, as a result of decompression, partial melting and ascent. These melts would have risen through a system of deep faults like the Gastre Fault System, following the last Quaternary glacial event.

Keywords: Patagonia; Holocene; Alkaline; Volcanism

1. Introduction

This paper characterizes the volcanism of a Quaternary basaltic field in northern Patagonia, establishes its tectonomagmatic evolution, to investigate its petrographic and chemical characteristics and to compare them with other Quaternary basaltic fields of Patagonia.

The Crater Basalt Volcanic Field (CBVF) is located to the northwest of the Chubut and southeast of the Rio Negro Provinces (Fig. 1), between 41°51′ and 42°14′S and 69°44′ and 70°30′W.

The Cenozoic–Recent volcanism in northern Patagonia is restricted to the Andean magmatic arc and, in the extra-Andean area, to the Somuncura region. In southern Patagonia, the Quaternary volcanism is related to slab window formation (Ramos and Kay, 1992; D'Orazio et al., 2000; Gorring et al., 2003).

The origin of CBVF displays an interesting enigma: CBVF basalts were erupted in close proximity to the Somuncura basalts, though about 26 Ma later. In

* Corresponding author. Centro Nacional Patagónico, CONICET, Bvd. Brown 3500, 9120 Puerto Madryn, Argentina. Tel.: +54 2965 451024; fax: +54 2965 451543.
E-mail addresses: gim@cenpat.edu.ar (G.I. Massaferro), haller@cenpat.edu.ar (M.J. Haller).
[1] Fax: +54 2965 451543.

0377-0273/$ - see front matter © 2006 Published by Elsevier B.V.
doi:10.1016/j.jvolgeores.2006.02.002

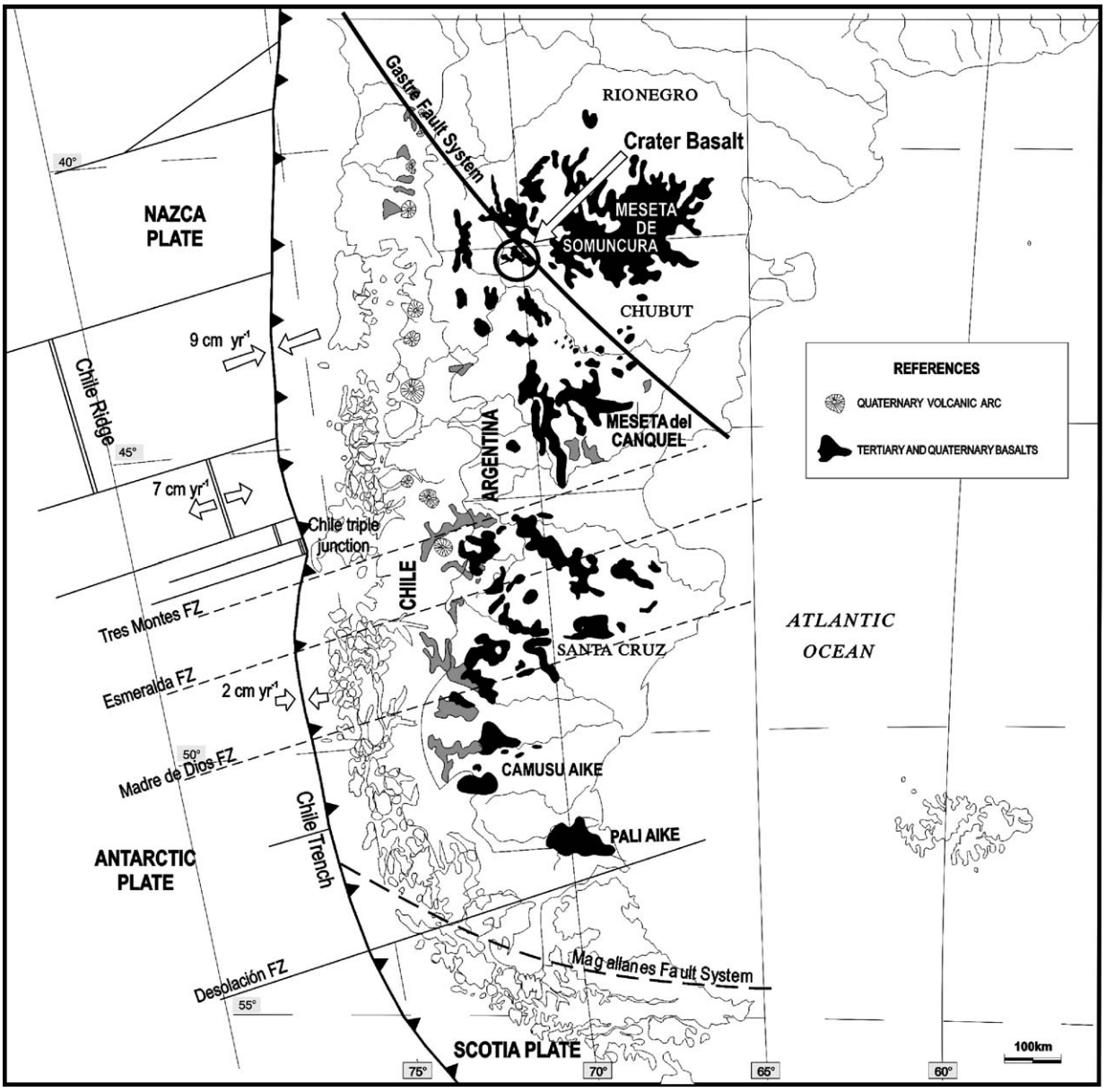

Fig. 1. Tertiary–Quaternary volcanism distribution in Patagonia. Sketch of the present tectonic configuration of Pacific and South American plates, location of GFS in relation to CBVF and other outcrops.

addition, the CBVF show strong chemical affinities with the basaltic plateaus of southern Patagonia. There is no evidence to propose an asthenospheric slab window below the area of CBVF or even Somuncura, or to relate these areas to the Andean magmatic arc.

There are few previous studies about CBVF volcanism. Ravazzoli and Sessana (1977) and Volkheimer (1964) described the regional geology. More recently Haller (2000), Haller et al. (2001) and Massaferro et al. (2002) described some petrographic features of the volcanic products. Haller (2004) describes eruption mechanisms in this volcanic field.

2. Geotectonic framework

The setting of CBVF in relation with other Tertiary–Quaternary basaltic outcrops in Patagonia within the present geodynamic framework is shown in Fig. 1.

The Meseta de Somuncura, an important Late Oligocene–Early Miocene volcanic complex, is located

to the northeast of CBVF. This complex, the largest Patagonian volcanic pile (Kay et al., 1993), is mainly composed of mafic lavas of tholeitic and alkaline affinities (Remesal and Parica, 1989; Kay et al., 1993). The origin of this complex remains uncertain. Kay et al. (1993) attributed this volcanism to a transient, hot spot-like anomaly, whereas Muñoz et al. (2000) and de Ignacio et al. (2001) related it to a slab roll back process.

There are other outcrops of Upper Cretaceous and Miocene basalts, covered by Plio-Quaternary lavas constituting the Meseta de Canquel 250 km southwards CBVF. According to Stern et al. (1990) and Alric (1996) these volcanic fields were formed from enriched asthenosphere melted in response to extensional efforts and crustal thinning. Southwards, in the Santa Cruz Province, there are many other volcanic fields with similar characteristics (e.g. Meseta del Lago Buenos Aires, Pali Aike, Camusú Aike) but they have been related to the subduction of segments of the Chile ridge beneath the Chile trench, opening an asthenospheric slab window (Ramos and Kay, 1992; Gorring et al., 1997; D'Orazio et al., 2000, 2005). At least two mid ocean ridge systems have collided in this region in Paleocene–Eocene and in the Neogene–Quaternary (Cande and Leslie, 1986).

The most important tectonic units recognized at the latitude of CBVF are:

(1) The Pacific archipelago, composed of metamorphic and sedimentary Paleozoic rocks intruded by calc-alkaline Jurassic to Tertiary plutons of the Patagonian Batholith.
(2) The Andean range, formed by Jurassic and Cretaceous volcaniclastic series and Tithono-Neocomian sediments, intruded by Cretaceous calc-alkaline plutons and covered by Paleogene calc-alkaline volcanics.
(3) The Chubut Precordillera, consisting of Carboniferous and Liassic sedimentary rocks, Liassic gabbroic and granite plutons and Tertiary volcanics.
(4) The Patagonian Jurassic rhyolitic plateau, overlain by the Tertiary Somuncura basaltic plateau.
(5) The central volcanoes Yanes, Hualaihue, Hornopirén and Huequi, located about 170 km to the West of the CBVF, represent the active calc-alkaline arc volcanism.

The CBVF lays about 400 km eastward of the current Peru–Chile Trench, where the Nazca Plate is subducting beneath the South American Plate at a rate of 9 cm per year, with a moderate oblique component (Hervé et al., 2000). This oblique convergence induces a dextral stress along the active volcanic arc, activating the Liquiñe–Ofqui fault system (Cembrano and Hervé, 1993). The current subducting plate is relatively young, ~10 Ma, (the actual age of the Nazca plate now entering the Chile trench at the latitudes 41° to 43°S is 15–20 Ma) making it light and buoyant. As Somuncura basalts are considered to be of Paleogene retroarc setting, the CBVF

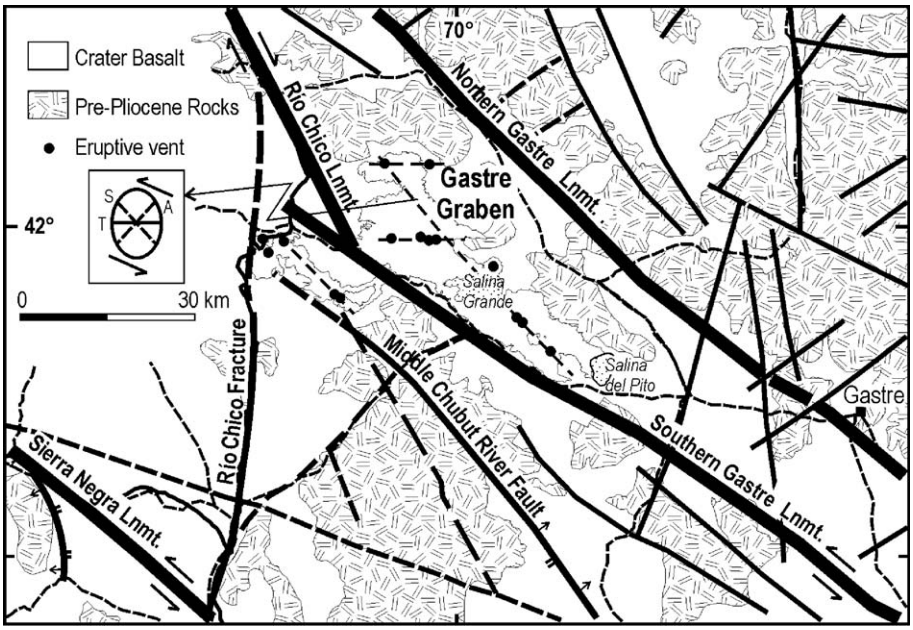

Fig. 2. Regional analysis of the field of stress in the area of Gastre graben.

Table 1
Major- and trace-element data for lavas from the Crater Basalt Volcanic Field

Sample	GA 3	GA 3E	GA 18A	GA 23	GA 29	GA 29/R	GA 32	GA 34	GA 36	GA 40	GA 43
Class.	AB	B	H	H	PT	PT	H	H	B	H	H
Lat. south	42°03′16″	42°03′16″	42°11′12″	42°13′42″	42°03′09″	42°03′09″	41°54′31″	41°54′39″	41°54′29″	42°06′44″	42°00′34″
Long. west	69°59′56″	69°59′56″	69°51′52″	69°49′09″	70°09′25″	70°09′25″	70°14′08″	70°13′12″	70°07′25″	70°13′21″	70°11′07″
Major elements (wt.%)											
SiO_2	49.94	47.66	47.19	48.50	48.73	48.77	48.34	48.88	46.52	48.66	49.27
TiO_2	1.75	2.22	2.01	1.95	2.09	2.09	2.03	1.91	2.09	1.90	1.93
Al_2O_3	16.30	15.97	15.41	15.99	15.86	15.85	15.30	15.54	15.14	15.76	16.71
Fe_2O_3 tot	10.98	11.25	11.33	11.57	11.21	11.24	11.77	11.05	12.48	11.14	10.70
MnO	0.15	0.15	0.15	0.15	0.15	0.15	0.15	0.14	0.17	0.16	0.14
MgO	6.97	7.50	7.86	7.60	8.10	8.16	8.68	7.94	9.01	8.73	6.45
CaO	9.05	7.37	8.82	8.94	7.87	7.89	8.02	7.78	8.58	8.23	8.79
Na_2O	3.80	4.56	3.92	3.90	3.89	3.88	4.19	4.12	3.92	3.75	4.25
K_2O	1.20	2.55	1.81	1.59	2.09	2.08	1.95	1.91	2.04	1.62	1.82
P_2O_5	0.52	0.71	0.50	0.43	0.53	0.54	0.58	0.49	0.58	0.45	0.50
L.O.I.	−0.17	0.36	1.20	−0.24	−0.15	−0.15	−0.53	0.23	−0.46	−0.04	−0.27
Tot.	100.49	100.30	100.20	100.38	100.38	100.50	100.49	100.00	100.06	100.36	100.29
Mg#	60	61	62	61	63	63	63	63	63	65	58
Trace elements (ppm)											
V	196	161	186	196	184	187	177	156	202	169	186
Cr	260	178	212	268	213	219	237	248	244	265	170
Co	41	43	41	43	42	45	44	42	49	43	34
Ni	25	67	60	33	70	74	79	174	83	99	23
Cu	28	45	36	37	34	35	38	36	45	42	34
Zn	102	106	95	93	88	99	97	94	100	95	77
Ga	22.3	23.2	20.2	21.1	21.1	21.9	21.3	21.1	22.2	20.0	20.4
Rb	21.9	55	35	30.9	45	48	44	41	43	30.0	37
Sr	495	764	611	587	671	682	675	631	699	593	621
Y	21.9	23.0	22.9	22.4	24.7	24.8	22.7	21.7	23.8	21.4	22.0
Zr	135	228	163	155	187	197	187	180	202	162	163
Nb	15.0	45	29.6	25.1	36	38	37	32.2	43	28.3	25.5
Cs	<d.l.	0.66	0.58	0.50	0.74	0.81	0.80	0.77	0.65	<d.l.	0.71
Ba	294	578	366	339	472	492	445	406	440	387	341
La	17.7	41	28.9	23.2	33	31.7	34	29.5	35	27.8	25.9
Ce	37	75	56	47	65	63	64	57	66	54	52
Pr	4.4	8.3	6.3	5.5	7.3	7.3	7.2	6.5	7.5	6.1	5.9
Nd	19.7	36	28.4	24.6	31.8	31.2	31.7	28.6	32.3	26.6	26.4
Sm	4.6	6.7	6.1	5.3	6.7	6.3	6.5	5.9	6.3	5.7	5.8
Eu	1.54	2.09	1.88	1.75	2.02	1.96	1.97	1.83	1.98	1.81	1.78
Gd	4.7	6.3	5.7	5.1	6.0	5.9	5.7	5.4	5.8	5.2	5.2
Tb	0.72	0.88	0.86	0.76	0.89	0.86	0.84	0.79	0.85	0.80	0.81
Dy	3.8	4.3	4.5	4.1	4.6	4.4	4.2	4.1	4.3	4.2	4.2
Ho	0.75	0.78	0.83	0.77	0.84	0.83	0.77	0.74	0.81	0.75	0.76
Er	2.13	2.19	2.34	2.19	2.40	2.37	2.23	2.17	2.31	2.18	2.25
Tm	0.30	0.28	0.32	0.30	0.34	0.31	0.30	0.29	0.30	0.29	0.31
Yb	1.65	1.57	1.74	1.64	1.83	1.79	1.61	1.56	1.65	1.69	1.68
Lu	0.23	0.18	0.24	0.23	0.24	0.24	0.20	0.20	0.22	0.20	0.23
Hf	3.3	5.1	4.3	3.7	4.7	4.6	4.6	4.5	4.7	4.0	4.2
Ta	–	–	–	–	–	–	–	–	–	–	–
Th	2.03	4.6	3.12	2.57	3.9	3.8	3.9	3.5	3.7	3.06	3.10
U	0.57	2.31	0.92	0.83	1.18	1.13	1.18	1.04	1.10	0.68	0.93
$^{87}Sr/^{86}Sr$								0.704777			

AB, alkali basalt; B, basanite; H, hawaiite; PT, potassic trachybasalt. "-", not determined. L.O.I., loss on ignition as loss on ignition as measured. Mg#=Mg/(Mg+Fe2+)*100 assuming Fe2O3 wt.%/FeO wt.%=0.20. Localities: Cerro Ventana (GA 3, 3E), Cerro García (GA 18A, 23), Cerro Fermín (GA 29, 29/R, 43), Cerro Volcán (GA 32, 34), Loma Gaucha (GA 36), Cerro Negro (GA 40, 55, 56, 57, 58), Cerro Antitruz (GA 47, 48L, 48B), Cerro Pinchuleu(GA 53), Cerro Pinchuleu flow (GA 49, 51).

GA 47	GA 48L	GA 48B	GA 49	GA 51	GA 53	GA 55	GA 56	GA 57	GA 58
B	B	B	PT	B	PT	PT	PT	PT	PT
42°03′29″	42°11′12″	42°51′48″	42°14′02″	42°08′24″	42°08′37″	42°07′46″	42°08′46″	42°08′59″	42°06′18″
70°25′55″	69°51′52″	69°51′48″	69°50′53″	69°55′52″	69°55′17″	70°13′23″	70°16′46″	70°15′59″	70°13′28″
46.57	45.34	45.61	47.78	46.58	47.03	48.14	47.68	47.84	47.55
2.28	2.17	2.28	1.54	2.46	1.87	1.62	1.96	1.98	1.74
16.02	15.46	15.71	15.41	14.98	14.97	15.01	16.63	16.64	15.55
11.97	12.01	11.90	11.10	11.39	11.65	11.06	10.57	10.45	10.83
0.16	0.16	0.16	0.15	0.15	0.15	0.14	0.14	0.14	0.14
8.20	8.04	8.14	7.83	7.81	8.36	8.85	6.32	6.26	7.80
8.17	7.93	8.10	9.07	8.14	8.75	8.10	8.89	8.92	8.91
4.50	4.35	4.34	3.45	4.05	3.42	3.44	3.95	3.95	3.59
2.38	2.31	2.41	2.01	2.53	2.15	2.01	2.22	2.26	2.04
0.63	0.64	0.65	0.42	0.62	0.51	0.41	0.51	0.53	0.42
−0.65	0.73	−0.22	0.40	0.07	0.53	−0.14	0.18	−0.05	0.49
100.23	99.14	99.08	99.16	98.78	99.39	98.64	99.05	98.92	99.06
62	61	62	62	62	63	65	58	58	63
179	175	183	203	180	183	181	207	204	201
144	144	136	271	186	210	289	139	149	262
42	72	45	43	43	46	46	36	35	42
50	53	51	109	145	161	198	67	64	113
36	58	34	47	47	48	57	41	44	50
81	97	95	–	–	–	–	–	–	–
20.8	21.5	22.5	19.4	20.8	19.6	19.1	20.8	21.1	19.3
46	48	50	28.1	48	35	29.7	37	37	31.0
754	747	794	594	775	667	597	729	742	629
23.5	24.1	23.5	22.1	24.4	23.7	21.2	24.3	24.2	21.1
204	214	215	151	231	187	167	194	198	166
37	37	40	27.8	52	39	30.2	40	40	29.5
0.94	1.03	0.99	0.47	0.83	0.45	0.45	0.72	0.64	0.54
491	488	504	355	526	467	376	421	446	347
36	35	37	21.9	39	31.7	24.9	31.5	31.7	23.9
71	71	72	45	76	63	50	62	63	48
8.1	8.0	8.3	5.7	9.1	7.7	6.2	7.6	7.7	6.0
35	34	36	23.7	36	30.2	25.4	31.2	31.2	24.7
7.2	6.9	7.2	5.4	7.6	6.3	5.6	6.4	6.6	5.4
2.18	2.13	2.14	1.68	2.28	2.16	1.64	2.13	1.93	1.61
6.3	6.0	6.3	4.9	6.5	5.6	5.0	5.9	5.9	4.9
0.89	0.87	0.92	0.78	0.97	0.88	0.78	0.89	0.90	0.76
4.5	4.6	4.6	4.2	5.1	4.6	4.3	4.7	4.7	4.0
0.81	0.85	0.82	0.81	0.90	0.90	0.77	0.88	0.87	0.81
2.32	2.37	2.35	1.97	2.10	2.01	1.85	2.15	2.07	1.81
0.31	0.32	0.30	0.27	0.27	0.28	0.26	0.29	0.29	0.24
1.73	1.81	1.67	1.57	1.66	1.60	1.63	1.78	1.70	1.53
0.21	0.24	0.21	0.22	0.22	0.22	0.21	0.25	0.26	0.21
5.1	5.0	5.3	3.7	5.2	4.3	3.7	4.5	4.5	3.7
–	–	–	1.73	3.30	2.48	1.89	2.38	2.42	1.82
4.3	4.3	4.4	2.80	5.0	4.0	3.24	3.9	4.0	3.04
1.42	1.38	1.40	0.75	1.40	1.07	0.75	1.02	1.03	0.82
0.704251									

is considered to correspond to the present retroarc region (Kay et al., 1993).

3. Structural framework

The occurrence of the CBVF is related to a very significant tectonic feature, the Gastre Fault System (GFS) (Fig. 1). This NE–SE fracture system, extends from the Pacific coast at 38°S to the Atlantic Ocean, at 45°S, separating two different geological domains. Its importance was pointed out by Rapela and Pankhurst (1992). Following these authors the GFS has preceded the Gondwana break-up.

The Northwest fractures delimit the Gastre trench, which is 30 km wide and similar strike (Fig. 2) and holds several playa (saline) lakes or *salinas*, such as Salina Grande, del Pito and del Molle. Most of the lava flows of the CBVF were extruded out within the Gastre trench. Other eruptive centers are located in the southwest limit of the graben.

The kinematics of the fault systems that affected the rocks of the region was studied by Coira et al. (1975) who concluded that the GFS behaved as a sinistral transcurrent fault during Late Mesozoic and Cenozoic times. Recently, von Gosen and Loske (2004) proposed a down faulting system as the origin of the Gastre fractures. Significant movements occurred during upper Cretaceous, with reactivations in late Neogene and Quaternary.

The main structural elements of Gastre area are shown in Fig. 2. Assuming a simple shear deformation, the eruptive centers are aligned following the tension and synthetic shear fault directions of an ideal deformation ellipse. Although the synthetic shear faults do not constitute a primary tensional system, they are zones of crust weakness that eventually can behave as tension fractures during an episode of compressional release.

The occurrence of Quaternary effusive centers closely related with the GFS, suggests that this segment of the fracture system delimited a transtensional trench during Neogene–Quaternary times.

4. Analytical methods

Twenty one representative samples of the CBVF have been analyzed for mayor and trace elements by ICP-MS in Actlabs. LTD, Ontario (from GA3 to GA48B), and in the Dipartimento di Scienze della Terra, Universitá di Pisa, Italy (GA49 to GA 58) (Table 1).

Mineral chemistry (Table 2) was determined by JEOL JXA-8600 electron microprobe (see Vaggelli et al., 1999 for details) at the CNR, Istituto di Geoscienze e Georisorse, Firenze, Italy, using Bence and Albee (1968) matrix correction procedure. Operative setting were 15 kV accelerating voltage, 10 nA cup current and 2 μm beam diameter beam spot. Standards used were natural silicate minerals and glasses.

Sr isotopes were measured in multi-dynamic mode on a ThermoFinnigan MAT triton-Ti nine-collector mass spectrometer at the Istituto di Geoscienze e Georisorse (C.N.R., Florence), and following conventional ion exchange methods for Sr separation. Five collectors were used for Sr analyses, and the mass fractionation effects were corrected for, with an exponential law, to $^{88}Sr/^{86}Sr=8.375209$. Repeated analyses of NIST SRM 987 ($SrCO_3$) yielded values of $^{87}Sr/^{86}Sr=0.710249\pm10$ ($n=22$).

5. Crater Basalt Volcanic Field

5.1. Volcanic features

The CBVF has an elongated form in the NW–SE direction, is 60 km length, and covers an area of 700 km^2. It includes nine main eruptive centers that erupted about 2.3 km^3 of lava (Fig. 3). The volcanic morphology is in general well preserved. Most of the vents are spatter or cinder cones. The flows are mainly pahoehoe-type and ranging in thickness from 1 to 10 m. Common features include tumulis or pressure ridges, and occasional coarse columnar jointing.

One of the most important eruptive centers, in terms of erupted volumes, is Cerro Fermín, an 1153 m high cinder cone. This volcano probably has more than one crater but the older structures have been eroded. It is composed by spatter, cinder and blocks. At its base are two black and massive blocky lava flows. Six different superimposed lava flows can be distinguished extruding from this center. Adjacent to Cerro Fermín, is a very well preserved cinder cone.

Pinchuleu and Contreras hills are typical cinder cones. Pinchuleu is 1005 m high and extruded at least four flows. Cerro Contreras (1004 m high) is deeply eroded, only two volcanic conduits are well preserved. Three different flows are associated with this center.

Cerro Ventana is a partially eroded spatter cone, 1008 m high. Seven flows have been recognized as originating from this cone; some of the flows are blocky-type aa flows and others are ropy-type pahoehoe flows. Bombs and cinders near the vent of the cone are very oxidized and vesicular, but at the base of cone, the blocks are black and less vesicular. The crater diameter is 450 m.

Cerro Volcán is a scoria cone, of 1025 m high, and has a main crater that is 100 m in diameter and 30 m deep with a

Table 2
Mineral chemistry for samples GA 43 and GA 57 (oxides weight percent and, in parentheses, standard deviations)

n	GA 43					GA 57					
	Olivine phenocryst	Olivine groundmass	Pyroxene groundmass	Ti-magnetite	Ilmenite	Olivine phenocryst	Olivine groundmass	Pyroxene groundmass	Ti-magnetite	Ilmenite	Cr-spinel
	2	1	1	4	4	8	4	2	4	4	4
SiO_2	38.8	38.1	50.0	0.12 (0.10)	0.05 (0.04)	39.8 (0.6)	36.8 (0.6)	46.8	0.17 (0.07)	0.66 (0.40)	0.10 (0.04)
TiO_2			1.36	23.3 (1.2)	48.8 (0.5)			2.79	23.8 (0.6)	48.3 (0.5)	2.98 (1.7)
Al_2O_3			5.21	1.79 (0.16)	0.08 (0.04)			5.92	2.61 (0.29)	0.31 (0.17)	27.6 (5.7)
FeO	22.1	27.0	6.30	67.7 (1.2)	46.4 (0.7)	17.8 (1.2)	26.9 (1.0)	8.36	66.7 (0.7)	43.9 (0.4)	34.4 (5.7)
MnO	0.33	0.44	0.15	0.58 (0.06)	0.79 (0.08)	0.25 (0.04)	0.44 (0.04)	0.13	0.65 (0.04)	0.81 (0.10)	0.24 (0.03)
MgO	39.6	35.8	14.7	1.79 (0.14)	1.11 (0.34)	43.2 (1.1)	33.2 (2.6)	12.7	1.79 (0.17)	1.63 (0.16)	11.3 (1.1)
CaO	0.28	0.43	21.8	0.14 (0.07)	0.12 (0.03)	0.27 (0.03)	0.67 (0.17)	21.8	0.19 (0.11)	0.21 (0.05)	<d.l.
NiO	0.12	0.08		<d.l.		0.12 (0.03)	0.08 (0.03)		<d.l.	<d.l.	0.09 (0.01)
Cr_2O_3	<d.l.	<d.l.	0.45	<d.l.	<d.l.	0.08 (0.06)	<d.l.	0.10	<d.l.	<d.l.	21.6 (1.5)
Na_2O			0.38					0.56			
Total	101.2	101.8	100.4	95.4	97.4	101.5	98.1	99.2	95.9	95.8	98.3
End-members	$Fo_{76.2}$	$Fo_{70.3}$	$Fs_{10.7}$ $Wo_{46.0}$	$Usp_{66.5\ (3.1)}$	$Ilm_{94.1\ (1.0)}$	$Fo_{81.2\ (1.4)}$	$Fo_{68.7}$	$Fs_{14.3}$ $Wo_{47.3}$	$Usp_{67.5\ (1.2)}$	$Ilm_{95.6\ (0.4)}$	Cr# 28.2 (0.4)

n, number of analyses; "<d.l.", below detection limit; "blank", not determined. End-members: Fo, forsterite; Fs, ferrosilite; Wo, wollastonite; Usp, ulvospinel; Ilm, ilmenite. Cr#, $Cr/(Cr+Fe^{3+}Al)$ *100. Analyses performed with a JEOL JXA-8600 electron microprobe at Istituto di Geoscienze e Georisorse, CNR, Florence, Italy. Operative setting were: 15 kV accelerating voltage, 10 nA cup current and 2 μm beam spot. Matrix correction procedure following Bence and Albee (1968). Calibration standards were natural silicate minerals and glasses.

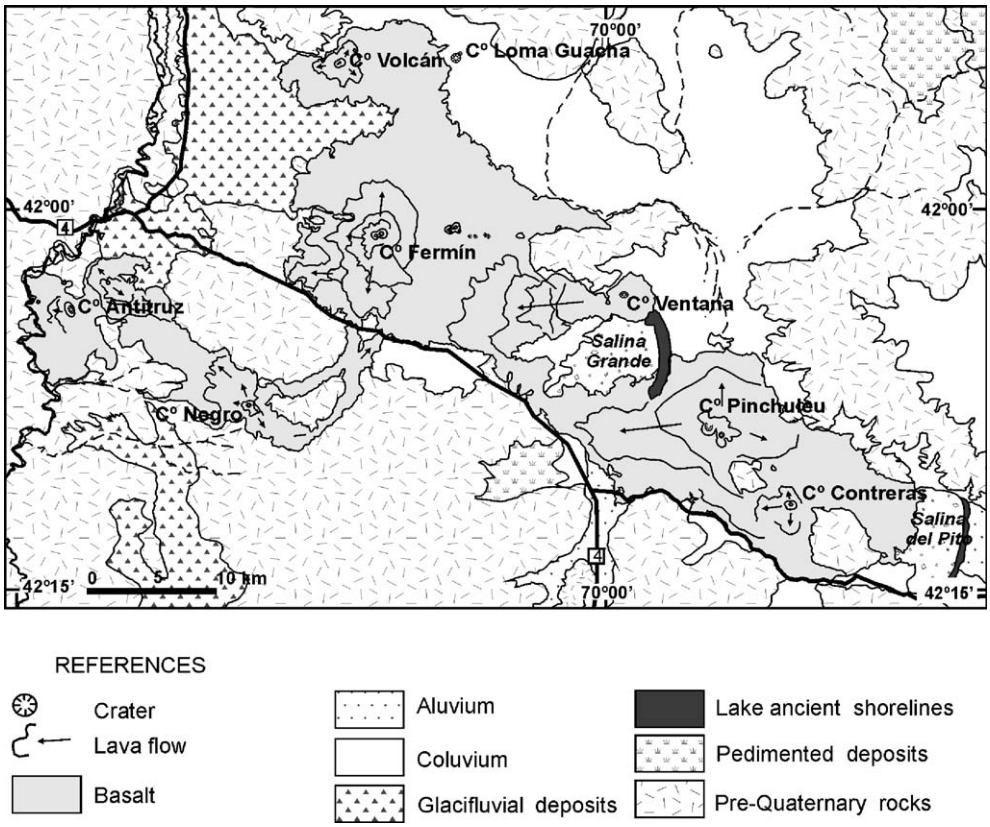

Fig. 3. Geological map of CBVF.

small nested cone developed on the west side of the crater. Three different flows originated from this cone, varying in thickness from 3 to 10 m. The Loma Guacha hill is located 3 km to the west, and have similar characteristics. Loma Huacha is a pyroclastic cone that is 959 m in height with a small parasitic cone on its northeast flank. The crater is about 50 m wide with a breach to the north. In certain sectors, the cinder fragments show a yellow patina (Fe-oxides?). The alluvial sediments of the Mamil Choique Creek cover the flows that originated from this center.

Two other main volcanic centers are located outside of the Gastre trench, over a structural high in the southwest part of the study area: Antitruz and Negro hills, and other minor cones.

Cerro Antitruz (1100 m high), located to the west of the volcanic field, is a pyroclastic cone with some different characteristics compared with the previously mentioned volcanoes. Lapillitic and coarse layers, stratified bombs and blocks, are exposed on one wall of the cone. Cerro Antitruz erupted blocks up to 5 m in height. Near the base of the volcano there are remnants of a conduit composed of vesicular, black, porphyritic lava. Three flows of lava are related to this volcano. To the northeast of Antitruz cone, there is another volcano that extruded 4 flows. Also, to the north and west, there are other small pyroclastic cones without associated flows.

Cerro Negro is the highest one of the volcanoes of the volcanic field reaching 1359 m in elevation, produced at least four blocky flows that flowed in channels to the west and the east and then to the north-east joining the flows of the Gastre trench, near provincial road 4.

It is possible to recognize some "windows" within the lava field: For example, basement rocks are exposed to the west of Cerro Negro. To the northwest and southwest of Pinchuleu hill, Jurassic sedimentary rocks of the Cañadón Asfalto Formation are exposed and to the southeast of Cerro Contreras there are outcrops of the Cretaceous sedimentary rocks of Chubut Group.

5.2. Stratigraphic relationships

The CBVF basaltic flows cover Quaternary river terraces, flow into valleys and also cover sub-recent clay and evaporite deposits in Salina Grande and Salina del Pito. In contrast, the alluvial sediments transported by

Mamil Choique creek cover the Loma Guacha volcanics. These relationships indicate that the eruption of these volcanics occurred during Holocene times.

Considering the field relationships and the erosion level of the volcanic features, it is possible to establish a relative chronology among the centers that compose the volcanic field. Antitruz volcano has a smoothed morphology that may be the result of deeper erosion than the other volcanoes however, the Cerro Negro flows cover those of Cerro Antitruz. Cerro Ventana is one of the youngest centers as its flows partially cover the recent alluvial fan of Mamil Choique creek and the Holocene coast ridges of Salina Grande playa lake. In a similar way, flows from Cerro Contreras cover clay-evaporite deposits of Salina del Pito.

In summary, a space–time evolution of the volcanic activity can be established: Antitruz and Loma Guacha volcanoes, located in the westernmost portion of CBVF, represent the older volcanic episodes. Later, the largest volume of lavas was produced from vents inside the Gastre trench, finally, the volcanic activity moved to the Ventana and Contreras hills. This succession of events indicates a migration with time of volcanic activity to the east.

6. Petrography and geochemistry

In general the basalts are black and vesicular, and some contain ultramafic xenoliths up to few millimeters in size. Most of the samples are porphyritic or microporhyritic in texture. The proportion of phenocrysts varies between 10 and 30 vol.%; and the phenocrysts are olivine only. The groundmass has an intergranular or intersertal texture (although fresh glass is rare) with varying grain size. Olivine phenocrysts (Fo_{75}–Fo_{84}) are euhedral to subhedral, fresh and fractured, and up to 3.5 mm in maximum length. They contain euhedral Cr-spinel inclusions. In the most glass-rich samples, olivine phenocrysts are embayed. The groundmass is mainly made of plagioclase (andesine–labradorite) microlites and subhedral green to purplish clinopyroxenes of diopside/augite composition (Table 2). Less abundant are subhedral microcrysts of olivine and opaques (Ti-magnetite and ilmenite; Table 2).

The ultramafic xenoliths are dunite and lherzolite with protogranular to porphyroclastic textures up to 4 mm in size. They consist of 60% olivine and enstatite, and opaques represent the rest of the phenocrysts. The olivine has hipidioblastic shape and incipient alteration to iddingsite in fractures and borders. It also contains spinel inclusions. Enstatite is xenoblastic, very fractured and colorless.

Samples from Cerro Volcán also host ellipsoidal xenoliths, which range in size from few millimeters up to 10 cm. These xenoliths are composed of quartz and plagioclase surrounded by a reaction rim, and were probably derived from the Mamil Choique igneous–metamorphic rocks that constitute the basement of the region.

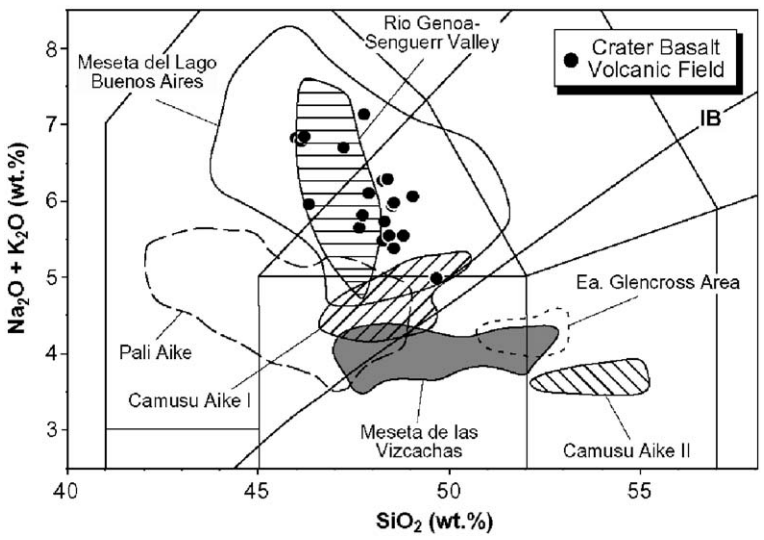

Fig. 4. Total alkali vs. silica diagram (Le Maitre, 1989) for the studied rocks. The fields for other Miocene to Pleistocene lavas from central and southern Patagonia are also shown for comparative purposes. Data sources: Pali Aike (D'Orazio et al., 2000); Camusú Aike, (D'Orazio et al., 2005); Río Genoa-Senguerr (Bruni, 2003); Ea. Glencross Area (D'Orazio et al., 2001); Meseta de las Vizcachas (author's unpublished data); Meseta del Lago Buenos Aires post-plateau lavas (Gorring et al., 2003). The boundary line (marked IB) between alkaline and subalkaline rocks of Irvine and Baragar (1971) is also plotted.

Some flows show minor differences with respect to the most abundant basalt types. For example, the basalts from Loma Guacha hill have clinopyroxene phenocrysts and orthopyroxene xenocrysts with reaction rims.

Twenty one volcanic rock samples, representative of the CBVF, were analyzed for major and trace elements (Table 1). The CBVF rocks are trachybasalts (both hawaiites and potassic trachybasalts), basanites and basalts based on the total alkali vs. silica diagram (TAS; Le Maitre, 1989) (Fig. 4). All samples are nepheline normative (ne=1–13 wt.%) and have >13 wt.% of normative olivine. The basalts are relatively primitive with high values for the Mg# (58–65) and the high contents of MgO (6–9 wt.%), Cr (136–289 ppm), Ni (25–198 ppm) and Co (34–72 ppm). In the Harker type diagrams, using MgO as differentiation index (Fig. 5), Fe_2O_3 shows a positive correlation, while Al_2O_3 show negative slope. CaO and K_2O_5 show constant values against MgO. Minor elements like Cr and Ni display general positive trends. All these arguments may suggest small fractionation of olivine and magnetite. There is a slight negative correlation between alkalis (Na_2O+K_2O) and SiO_2 (Fig. 4). The two extreme samples (GA 3 and GA 3 E) have very similar Mg# (60 and 61, respectively). This could indicate that the chemical variability is related

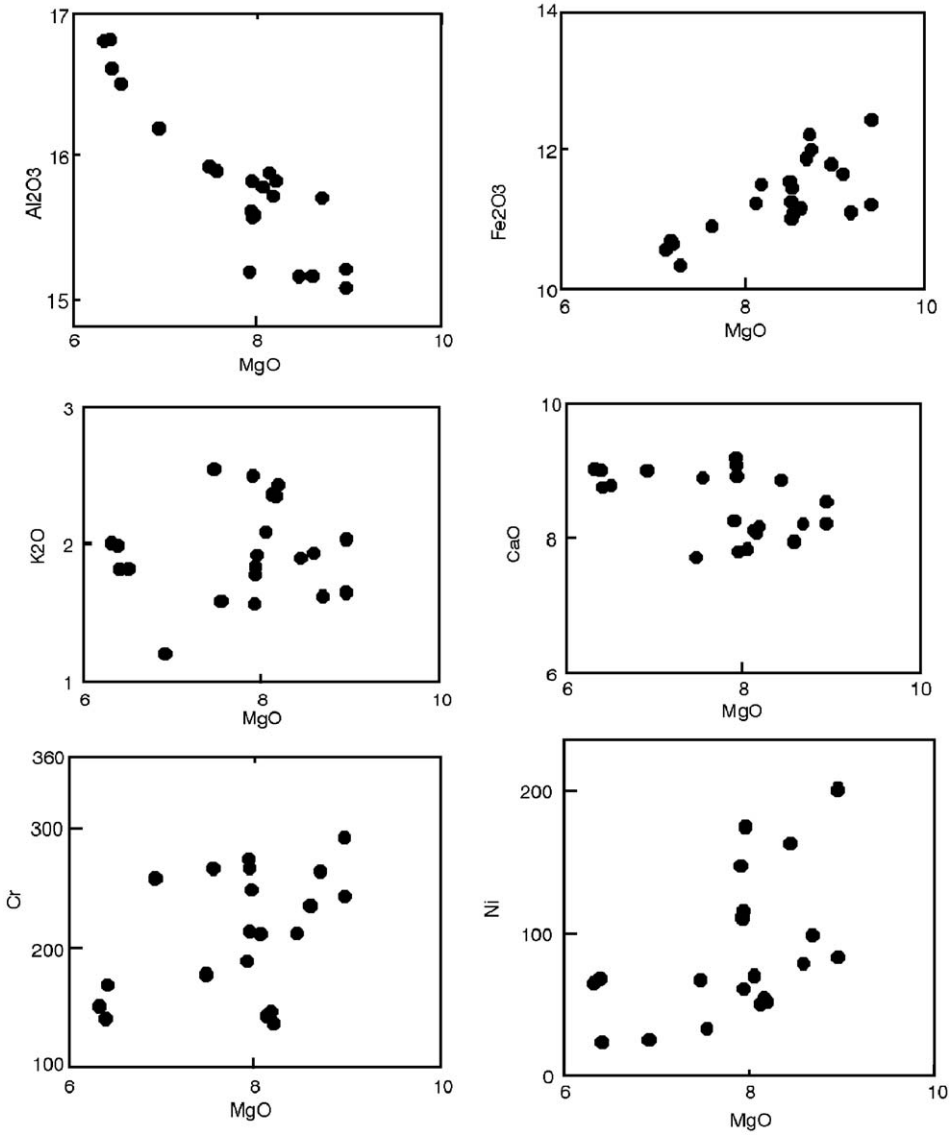

Fig. 5. Harker type diagram for CBVF samples. Oxides vs. MgO in weight percent. Trace element in parts per million.

more to the degree of melting than to the extent of crystal fractionation.

The incompatible element distribution of CBVF lavas is typical of basaltic magmas from within-plate settings (Fig. 6). Most Cenozoic alkaline lavas from the extra-Andean Patagonia show similar distributions of the incompatible elements, though slightly more enriched. Rare earth elements (REE) patterns are roughly rectilinear LREE enriched ($[La/Yb]_N$=7.3–16.0), similar to the majority of the Cenozoic alkaline Patagonian lavas (Fig. 7).

Two samples (GA 34 and GA 47) were analized for Sr isotope composition (Istituto di Geoscienze e Georisorse, C.N.R., Florence). The measured $^{87}Sr/^{86}Sr$ values (0.70478–0.70425) fall within the wide range defined by the entire Cenozoic Patagonian volcanic province (Fig. 8) and very close to those observed for the basalts of the Somuncura Fm. (Oligocene) and Quiñelaf Fm. (Middle Miocene) from Meseta de Somuncura (Kay et al., 1993).

In summary, the geochemical features of the CBVF basaltic rocks are similar to those of most Cenozoic alkaline lavas of the extra-Andean Patagonia occurring to the south. In particular, the radiogenic Sr isotope composition of CBVF lavas is closer to the Patagonian lavas occurring to the north of the latitude 50°S than to the isotopically depleted volcanic rocks exposed in southernmost Patagonia (i.e. Pali Aike, Estancia Glencross Area, Camusú Aike, Meseta de las Vizcachas).

7. Geothermometry

Phenocrysts of olivine and Cr-spinel (included in olivine), and groundmass crystals of olivine, clinopyroxene and Fe–Ti oxides (ilmenite and Ti-magnetite) were analyzed by microprobe (Table 2) in two lava samples (GA 43 and GA 57) from two representative cones (Cerro Fermín and Cerro Negro). These data

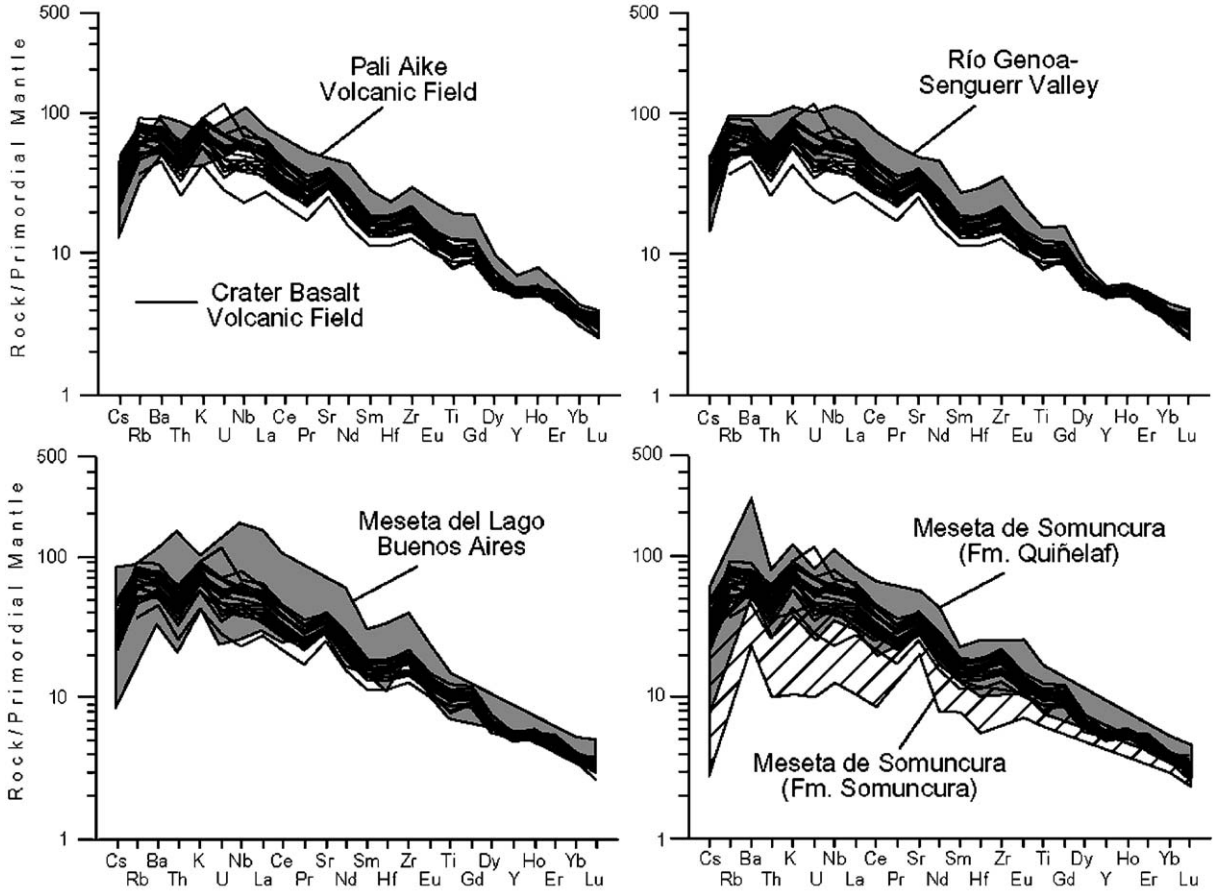

Fig. 6. Primordial mantle-normalized incompatible element patterns for CBVF lavas compared to other Cenozoic lavas from the extra-Andean Patagonia. Data sources: Pali Aike (D'Orazio et al., 2000); Río Genoa-Senguerr (Bruni, 2003); Meseta del Lago Buenos Aires (Gorring et al., 2003); Meseta de Somuncura (Kay et al., 1993). Normalizing values after McDonough and Sun (1995).

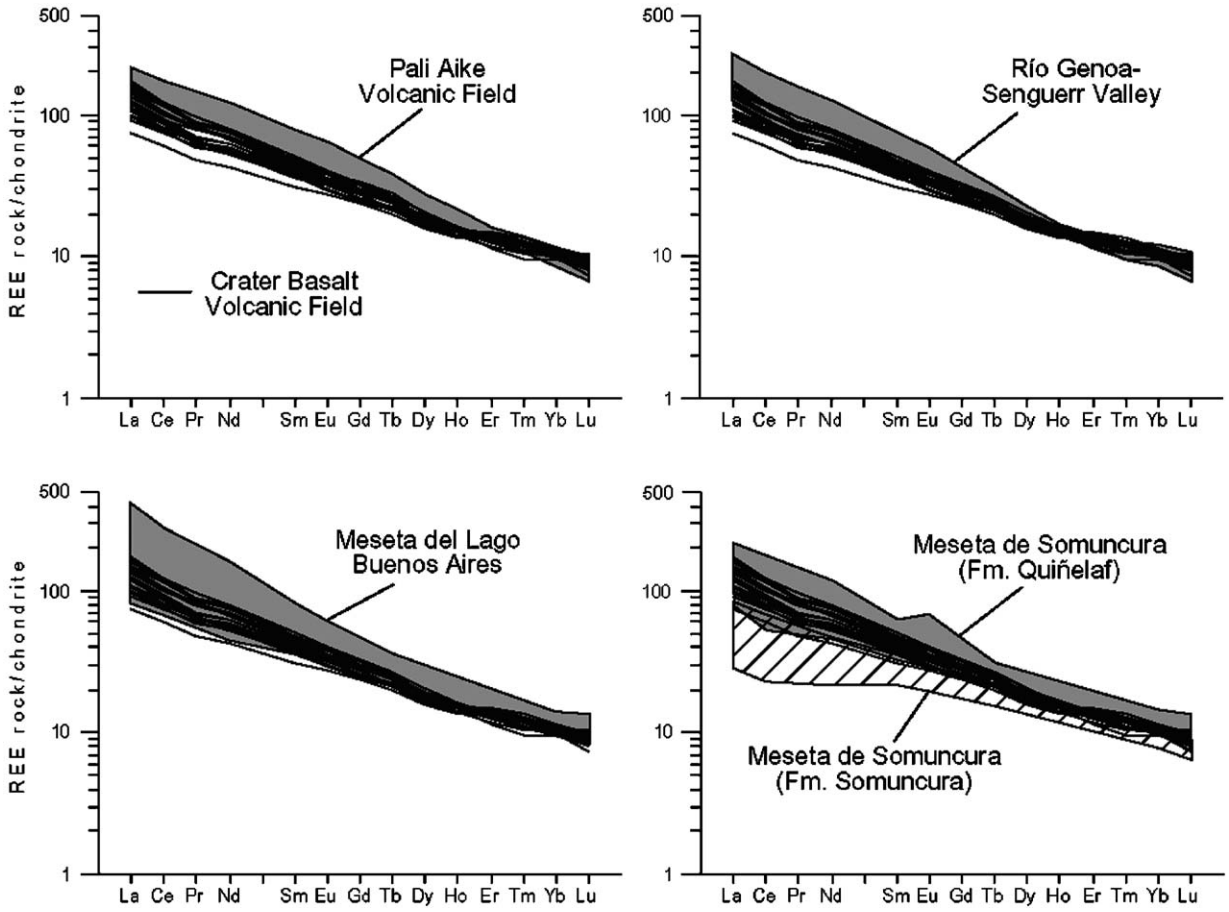

Fig. 7. CI chondrite-normalized REE patterns for CBVF lavas compared to other Cenozoic lavas from the extra-Andean Patagonia. Data sources as in Fig. 5. Normalizing values after McDonough and Sun (1995).

were used to calculate equilibrium temperatures using existing geothermometers.

The Mg–Fe^{2+} cation exchange geothermometer of Loucks (1996) was applied to the pairs olivine–augite in equilibrium in the groundmass. Temperatures were also calculated using olivine–Cr–spinel (Sack and Ghiorso, 1991), ilmenite–magnetite (Ghiorso and Sack, 1991) and olivine–liquid equilibria (Leeman and Scheidegger, 1977) (Table 3).

The highest estimated temperatures (~1135 °C) are related to the olivine–liquid equilibrium and should be closer to the liquidus temperature. Temperatures calculated using the Fe–Ti oxides geothermometer (855–960 °C) could indicate the groundmass temperature of crystallization (solidus), but the lowest temperatures may also correspond to sub solidus re-equilibration temperatures. The coexistence of Ti–magnetite and ilmenite makes it possible to calculate the fO_2 values, which vary from −1.0 to 0.0 (log△·FMQ values; Table 3).

8. Discussion

8.1. Role of crustal contamination and subduction-related components

Notwithstanding the relatively high $^{87}Sr/^{86}Sr$ values of the CBVF lavas, the rare occurrence of xenoliths of upper continental crust in some of the lavas, and the full continental setting of this magmatism behind an active continental arc, we found no detectable evidence neither of crustal contamination processes nor of the occurrence of subduction-related components. Indeed, all the analyzed CBVF lavas show low LILE/HFSE, low LREE/HFSE and low Ba/La ratios, similar to the large majority of primitive lavas from the extra-Andean Patagonia farther to the south. Moreover the $^{87}Sr/^{86}Sr$ values of CBVF lavas are comparable to, or just slightly higher than those measured on highly primitive uncontaminated lavas from other Patagonian volcanic areas.

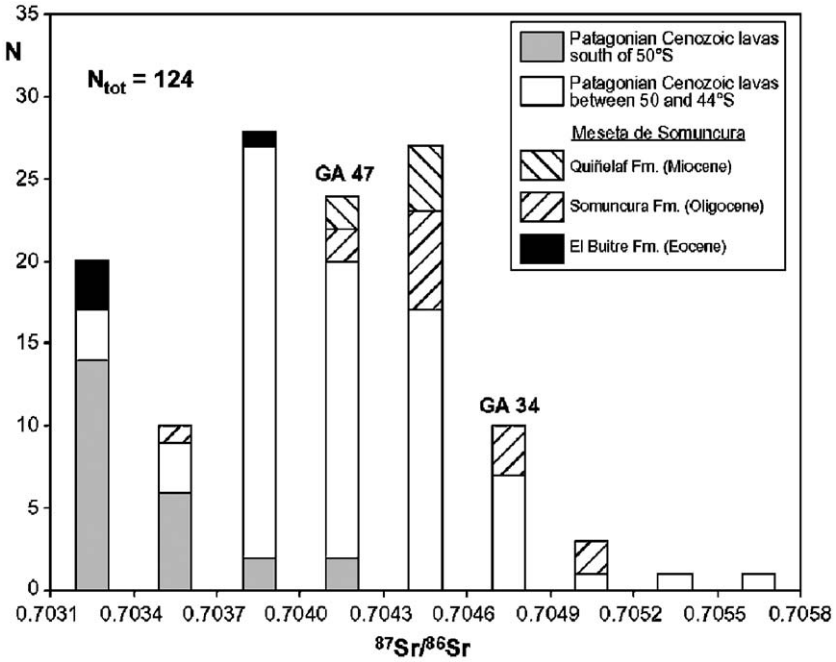

Fig. 8. Distribution of $^{87}Sr/^{86}Sr$ values for the Cenozoic extra-Andean mafic lavas. Data from an extensive literature (see D'Orazio et al., 2004 for detailed references).

8.2. Degree of partial melting of CBVF magma source from REE modeling

The CBVF lavas, though characterized by reasonably high Mg#s and high contents of MgO, Cr, Co and Ni, do not represent primary mantle magma compositions. Before attempting to use their REE distribution to constrain the melting degree and the REE concentrations of the CBVF mantle source, we must correct the REE content of our samples for the effect of crystal fractionation occurred during the ascent of the primary magmas towards the surface. The primary magma compositions were approximated on the basis of the following assumptions: i) the primary magma

Table 3
Equilibrium temperature estimates for CBVF lavas

Sample	Pair	Geothermometer	Temperature (°C)	fO_2 ΔFMQ
GA 43	ol–cpx (groundmass)	Loucks (1996)	1025	
GA 57	ol–cpx (groundmass)	=	1055	
GA 57	ol–cpx (groundmass)	=	1100	
GA 43	ilm–mag (groundmass)	Ghiorso and Sack (1991)	855	0.0
GA 43	ilm–mag (groundmass)	=	930	−0.5
GA 43	ilm–mag (groundmass)	=	960	−0.2
GA 43	ilm–mag (groundmass)	=	865	−1.0
GA 57	ilm–mag (groundmass)	=	885	−1.0
GA 57	spl–ol (phenocryst)	Sack and Ghiorso (1991)	1040	
GA 57	spl–ol (phenocryst)	=	1010	
GA 57	spl–ol (phenocryst)	=	1075	
GA 57	spl–ol (phenocryst)	=	1085	
GA 57	spl–ol (phenocryst)	=	1055	
GA 57	spl–ol (phenocryst)	=	990	
GA 43	ol–liq (phenocryst)	Leeman and Scheidegger (1977)	1135	
GA 57	ol–liq (phenocryst)		1145	
GA 57	ol–liq (phenocryst)	=	1130	

Table 4
Melting modelling for CBVF primary magmas

	Grt-LHZ	Melting proportions[b]		Partition coefficients[c]	
	Source[a]	AB	B	La	Dy
Mode (weight fractions)					
Olivine	0.598	−0.141	−0.138	0.0004	0.0017
Orthopyroxene	0.211	0.403	0.447	0.0020	0.0220
Clinopyroxene	0.076	0.274	0.205	0.0540	0.3300
Garnet	0.115	0.464	0.486	0.0100	1.0600
	La	Dy			
Bulk D	0.0059	0.1526			
Bulk P (AB)	0.0202	0.5909			
Bulk P (B)	0.0168	0.5922			
Melting degree %		6.8	2.8		

[a]Garnet–lherzolite source of McKenzie and O'Nions (1991); [b]Melting proportions for CBVF alkali basalt (AB) and basanite (B) primary magmas calculated following the approach of Maaløe et al. (1992); [c]Mineral/melt partition coefficients for La and Dy of McKenzie and O'Nions (1991).

fractionated only olivine (the dominant phenocryst phase of CBVF lavas); ii) the K_D $(Fe/Mg)^{ol/liq}$ was taken as constant and equal to 0.30; iii) at the time of its segregation from the mantle, the primary magma was in equilibrium with mantle olivine Fo_{90}. The calculations were performed following the model proposed by Pearce (1978), continuously adding equilibrium olivine back to the magma until magma equilibrates with a mantle olivine Fo_{90}. The results of the calculation indicate the CBVF lavas required from 18 wt.% (GA 55) to 27 wt.% (GA 56) olivine to reach primary magma composition. Accordingly, the REE content of the samples was corrected for, assuming olivine contains negligible amounts of these elements.

The relative concentrations of the most incompatible elements of the CBVF lavas show no significant variation (Fig. 6). In addition, the observed LREE/HREE fractionation (Fig. 7) suggests the occurrence of garnet as a residual mantle phase. We can, therefore, hypothesize that the magmas erupted in the CBVF originated by variable degrees of melting of a garnet–lherzolite source with a homogeneous incompatible element composition. An approximate estimate of the degree of melting required to generate the CBVF magmas was made using the non-modal batch melting model (Shaw, 1970), and the concentration ratio method of (Maaløe, 1994) that does not require to make assumptions about source concentrations.

The REE, La and Dy, were selected for the calculations as they are determined with high precision by ICP-MS and their partition coefficients in mantle minerals are quite different and known with a good accuracy. The extreme CBVF compositions, corresponding to the basanitic and alkali basaltic primary magma end-members, have La=33.3, Dy=1.26 ppm and La=14.1, Dy=1.32 ppm, respectively. The proportions of the minerals entering the melt phase (Table 4) were estimated from the composition of the primary melts, following the approach of Maaløe et al. (1992). In the calculations (Table 4) we used the mineral/melt REE partition coefficients of McKenzie and O'Nions (1991). The results indicate a degree of melting of 6.8% for alkali basalt and 2.8% for basanite, respectively. These values are comparable to or slightly higher than those proposed for the alkali basalt-basanite from the post-plateau sequence of the Meseta del Lago Buenos Aires (degree of melting=1–5%; Gorring et al., 2003) and for the Pali Aike Volcanic Field and Estancia Glencross Area alkali basalt–basanite–subalkaline basalt (degree of melting=2–7%; D'Orazio et al., 2001). The REE concentration of the calculated CBVF source has a slightly concave-up shape (Fig. 9) with abundances from about 2.3 to 4.5 times chondritic values.

In summary, the REE modelling, notwithstanding its uncertainties and approximations, indicates that the chemical compositions of the CBVF lavas are compatible with a low to intermediate degrees of partial melting of a garnet–lherzolite source (depth>65 km) characterized by a roughly flat REE distribution at ~3× chondrite. In addition, the least enriched alkali basalt magma represents a degree of melting about twice that of the most enriched basanite magma.

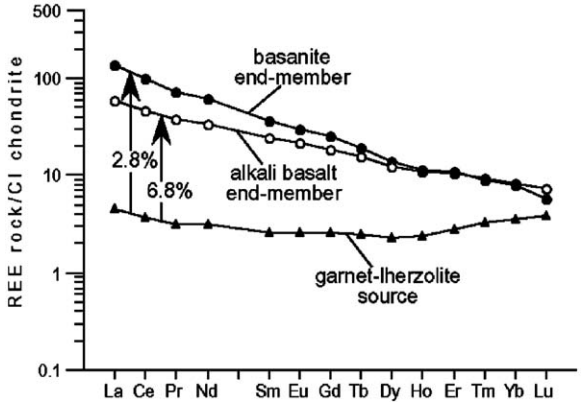

Fig. 9. CI chondrite-normalized REE patterns for the estimated mantle source of the CBVF magmas and for the two extreme calculated primary magma compositions. The numbers in percentage are the degrees of melting. Normalizing values after McDonough and Sun (1995).

8.3. Geodynamic significance of the CBVF

In the whole extra-Andean Patagonia region, the occurrence of a widespread and voluminous basaltic magmatism throughout the Cenozoic, poses two major questions: 1) how are mantle rocks melted in absence of a significant lithospheric extension?; and 2) why are most of the mantle sources of these magmas completely free of subduction-related geochemical imprints and yet occurring in a continental back-arc setting?

In the sector of Patagonia south of ~46.5°S these questions were convincingly addressed invoking the occurrence of a slab-window under this region of South America, originated by the Middle Miocene to present collision of the Chile Ridge with the Chile Trench (Ramos and Kay, 1992; Gorring et al., 1997; D'Orazio et al., 2000). The opening of a slab window can easily account for the melting of the uprising sub-slab asthenosphere by adiabatic decompression, and for the lack of subduction-related imprints in the magmas. Obviously, the opening of the Middle Miocene-present slab window in southern Patagonia does not have any relation with the basaltic rocks erupted before the Miocene in the same area and with the basalts erupted north of 46.5°S. Therefore, as regards the CBVF the two questions above require a different explanation.

Several hypotheses have been considered to explain the origin of these magmas. Stern et al. (1990) postulated that small amounts of extension in the back arc could generate crustal thinning, asthenospheric ascent and decompression. Similar to the origin of Somuncura Plateau (Kay et al., 1993) a small hot spot could also be considered. Another explanation of this volcanism could be the existence of small scale and short thermal anomalies associated to important lithosphere limits, called hot fingers (Wilson, 2003). Muñoz et al. (2000) postulate that in the late Oligocene, the southern margin of South America suffered moderate extension caused by increment in the rate of convergence between Nazca and South American plates. As a consequence, a slab roll back of the Nazca plate was induced.

Recently, de Ignacio et al. (2001) proposed an alternative to these interpretations for basalts from the Meseta de Somuncura. Namely that mantle melting under this area occurred in response to an enhanced and "channelized" corner flow of the asthenosphere in the mantle wedge. This, in turn, would be caused by a combination of slab roll-back and concave-up shape of the subducting plate. Though this model presents some problems, as the slab roll-back in this area contrasts with the general westward flow of plate motion (Doglioni et al., 1999) and the concave-up shape of the subducting plate has to be demonstrated, it could account for the creation of a "pure" asthenospheric mantle source for the subsequent magmatism of the nearby CBVF. The activation of this source during the Quaternary could be related to the occurrence of deep fractures, like the GFS, that would reach the base of the lithosphere inducing tectonic decompression and melting.

9. Conclusions

CBVF is a Holocene volcanic field of 700 km^2 in extent, composed by monogenetic volcanoes built by Hawaiian fountains-like eruptions. As a result of this activity, nine main eruptive centers have been recognized. They comprise cinder and spatter types which erupted about 2 km^3 of lavas. These lavas are vesicular and some carry ultramafic xenoliths. Mostly the samples show porphyritic or microporphyritic textures with only olivine (Fo_{75}–Fo_{84}) as phenocrysts. The groundmass may have intergranular or intersertal texture composed by plagioclase (andesine–labradorite) microlites and subhedral green to purplish clinopyroxenes, diopside/augite in composition.

The distribution of these centers, according to tectonic features related with GFS, added to the analysis of fracture systems, indicates the existence of a transtensional trench during the Quaternary in this area. The geochemical and isotopic compositions point out that the magmas were derived from an enriched garnet lherzolite mantle source of about 65 km depth, compatible with asthenospheric materials. Degrees of partial melting vary between by 6.8% to 2.8%. Only minor fractionation of olivine is indicated by major and trace elements trends.

Extension in the back arc region could generate crustal thinning, asthenospheric ascent and melting decompression tectonically induced by GFS, that propagated to the base of lithosphere. The asthenospheric ascent could also be the consequence of readjustment plate configuration (slab roll back). The lack of crustal contamination, as well as lack of homogenization of xenoliths indicate the absence of a magma chamber related to this volcanism and a rapid ascent through the crust, favored by the existence of deep fractures like GFS.

Acknowledgements

We are indebted to Nancy van Wagoner for critical reading of the manuscript and constructive suggestions. We thank Gloria Vaggeli for assistance in microprobe

analyses. We also want to thank to Giulia Perini for the Sr isotope determinations. To Matthew Gorring and anonymous reviewer for improving the manuscript. Financial support was provided through CONICET grant 2463/00. The Argentine–Italian Scientific Cooperation Program provided additional funds.

References

Alric, V., 1996. Los basaltos portadores de xenolitos aflorantes en las localidades Paso de Indios y cerro Cóndor, departamento de Paso de Indios, Provincia del Chubut. Thesis Doctoral. Universidad Nacional de la Patagonia San Juan Bosco. 135 pp.

Bence, A.E., Albee, A.L., 1968. Empirical correction factors for the electron microanalysis of silicate and oxides. Journal of Geology 76, 382–483.

Bruni, S., 2003. Le rocce ignee della Valle del Río Genoa-Senguerr e della catena del Cerro San Bernardo, Chubut, Argentina. Thesis, University of Pisa, Italy, 154 pp.

Cande, S., Leslie, R., 1986. Late Cenozoic tectonics of the southern Chile Trench. Journal of Geophysical Research 91 (B1), 471–496.

Cembrano, J., Hervé, F., 1993. The Liquiñe–Ofqui fault zone: a major Cenozoic strike-slip duplex in the southern Andes. Actas Interational Symposium of Andean Geodynamics, Oxford, vol. 2, pp. 175–178.

Coira, B., Franchi, M., Nullo, F., 1975. Vulcanismo del Terciario al oeste de Somuncura y su relación con el arco magmático de la Cordillera Nordpatagónica, Argentina. IV Congreso Geológico Chileno, Actas, vol. 4, pp. 68–88. Antofagasta.

de Ignacio, C., López, I., Oyarzun, R., Márquez, A., 2001. The northern Patagonia Somuncura plateau basalts: a product of slab-induced, shallow asthenospheric upwelling? Terra Nova 13, 117–121.

Doglioni, C., Harabaglia, P., Merlini, S., Mongelli, F., Peccerillo, A., Piromallo, C., 1999. Orogens and slabs vs. their direction of subduction. Earth Science Review 45, 167–208.

D'Orazio, M., Agostini, S., Mazzarini, F., Innocenti, F., Manetti, P., Haller, M., Lahsen, A., 2000. The Pali Aike volcanic field, Patagonia: slab-window magmatism near the tip of South America. Tectonophysics 321, 407–427.

D'Orazio, M., Agostini, S., Innocenti, F., Haller, M.J., Manetti, P., Mazzarini, F., 2001. Slab window-related magmatism from southernmost South America: the Late Miocene mafic volcanics from the Estancia Glencross area (~52°S Argentina–Chile). Lithos 57, 67–89.

D'Orazio, M., Innocenti, F., Manetti, P., Haller, M.J., 2004. The Cenozoic back-arc magmatism of the southern extra-Andean Patagonia (44.5–52°S): a review of geochemical data and geodynamic interpretations. Revista de la Asociación Geológica Argentina 59 (4), 525–538.

D'Orazio, M., Innocenti, F., Manetti, P., Haller, M.J., Di Vincenzo, G., Tonarini, S., 2005. The Late Pliocene mafic lavas from the Camusú Aike Volcanic Field (~50°S, Argentina): evidences for geochemical variability in slab window magmatism. Journal of South American Earth Science 18 (2), 107–124.

Ghiorso, M.S, Sack, R.O., 1991. Fe–Ti oxide geothermometry. Thermodynamic formulation and the estimation of intensive variables in silicic magmas. Contributions to Mineralogy and Petrology 108, 485–510.

Gorring, M.L., Kay, S.M., Zeitler, P.K., Ramos, V.A., Rubiolo, D., Fernandez, M.I., Panza, J.L., 1997. Neogene Patagonian plateau lavas: continental magmas associated with ridge collision at the Chile Triple Junction. Tectonics 16, 1–17.

Gorring, M.L., Singer, B., Gowers, J., Kay, S.M., 2003. Plio–Pleistocene basalts from the Meseta del Lago Buenos Aires, Argentina: evidence for asthenosphere–lithosphere interactions during slab window magmatism. Chemical Geology 193, 215–235.

Haller, M., 2000. Crater basalt: a back-arc postglacial volcanic event in northwestern Patagonia. Profil 18, 33 (4 págs).

Haller, M., 2004. Eruption mechanisms in the back-arc crater basalt volcanic field, Northern Patagonia. IAVCEI General Assembly. Abs. CD. Pucón.

Haller, M., Massaferro, G., Alric, V., 2001. Northwestern Patagonia Holocene basalts as indicators of an incipient continental fragmentation. Geoitalia 2001. 3° Forum Italiano di Scienze della Terra. Chietti, 5–8 Settembre. Sessione 19, 580–581.

Hervé, F., Demant, A., Ramos, V., Pankhurst, R., Suárez, M., 2000. The southern Andes. Tectonic Evolution of South America, International Geological Congress, pp. 605–634. Río de Janeiro.

Irvine, T.N., Baragar, W.R.A., 1971. A guide to the chemical classification of the common volcanic rocks. Canadian Journal of Earth Sciences 8, 523–548.

Kay, S., Ardolino, A., Franchi, M., Ramos, V., 1993. Origen de la meseta de Somun Cura: distribución y geoquímica de sus rocas volcánicas máficas. XII Congreso Geológico Argentino. Actas 4, 236–248 (Buenos Aires).

Leeman, W.P, Scheidegger, K.F., 1977. Olivine/liquid distribution coefficients and a test for crystal–liquid equilibrium. Earth and Planetary Science Letters 35, 247–257.

Le Maitre, R.W., 1989. A Classification of Igneous Rocks and Glossary of Terms. Recommendations of the International Union of Geological Sciences Subcommission on the Systematics of Igneous Rocks. Blackwell Scientific Publications, Oxford. 193 pp.

Loucks, R., 1996. A precise olivine–augite Mg–Fe exchange geothermometer. Contributions to Mineralogy and Petrology 125, 140–150.

Maaløe, S., 1994. Estimation of the degree of partial melting using concentration ratios. Geochimica et Cosmochimica Acta 58 (11), 2519–2525.

Maaløe, S., James, D., Smedley, P., Petersen, S., Garmann, L.B., 1992. The Koloa volcanic suite at Kauai, Hawaii. Journal of Petrology 33, 761–784.

Massaferro, G., Alric, V., Haller, M., 2002. El campo volcánico cuaternario del Basalto Cráter en la Patagonia Septentrional. XV Congreso Geológico Argentino. Actas II, 91–96.

McDonough, W.F., Sun, S.S., 1995. The composition of the Earth. Chemical Geology 120, 223–253.

McKenzie, D., O'Nions, R.K., 1991. Partial melt distributions from inversion of rare earth element concentrations. Journal of Petrology 32, 1021–1091.

Muñoz, J., Troncoso, R., Duhart, P., Crignola, P., Farmer, L., Stern, C., 2000. The Mid-Tertiary coastal magmatic belts in south-central Chile (36–43°S): it's relation to crustal extension, mantle upwelling and the late Oligocene increase in the rate of oceanic plate subduction beneath South America. Revista Geológica Chilena 27 (2), 177–203.

Pearce, T.H., 1978. Olivine fractionation equations for basaltic and ultrabasic liquids. Nature 276, 771–774.

Ramos, V., Kay, S., 1992. Southern Patagonian plateau basalts and deformation: backarc testimony of ridge collisions. Tectonophysics 205, 1–20.

Rapela, C., Pankhurst, R., 1992. The granites of northern Patagonia and the Gastre Fault System in relation to the break-up of Gondwana. In: Storey, B., Alabaster, T., Pankhurst, R. (Eds.), Magmatism and the Causes of Continental Break-up. Geological Society Special Publication, vol. 68.

Ravazzoli, I., Sessana, F., 1977. Descripción Geológica de la hoja 41c, Río Chico, pcia. de Río Negro. Boletín, vol. 148. Servicio Geológico Nacional.

Remesal, M., Parica, C., 1989. Caracterización geoquímica e isotópica de basaltos del sector noreste de la Meseta de Somuncurá. Revista de la Asociación Geológica Argentina 44 (1–4), 353–363.

Sack, R.O., Ghiorso, M.S., 1991. Chromian spinels as petrogenetic indicators; thermodynamics and petrological applications. American Mineralogist 76, 827–847.

Shaw, D., 1970. Trace element fractionation during anatexis. Geochimica et Cosmochimica. Acta 34, 237–243.

Stern, C., Frey, F., Futa, K., Zartman, R., Peng, Z., Kyser, T., 1990. Trace-element and Sr, Nd, Pb, and O isotopic composition of Pliocene and Quaternary alkali basalts of the Patagonian Plateau lavas of southernmost South America. Contributions to Mineralogy and Petrology 104, 294–308.

Vaggelli, G., Olmi, F., Conticelli, S., 1999. Quantitative electron microprobe analysis of reference silicate mineral and glass samples. Acta Vulcanologica 11 (2), 297–303.

Volkheimer, W., 1964. Observaciones geológicas en el área de Ingeniero Jacobacci y adyacencias (Provincia de Río Negro). Revista de Asociación Geológica Argentina 28 (1), 13–36.

von Gosen, W., Loske, W., 2004. Tectonic history of Calcatapul Formation, Chubut Province, Argentina, and the "Gastre Fault System". Journal of South American Earth Science 18, 73–88.

Wilson, M., 2003. The geodynamic setting of Tertiary–Quaternary intra-plate magmatism in Europe: the role of asthenospheric diapers for mantle "hotfingers". Penrose Plume IV Conference. Iceland. www.mantleplumes.org/Penrose/PenPDFAbstracts/Wilson_Marge_abs2.pdf (11-09-2003).